Cell

Rapid Microtubule Self-Assembly Kinetics

Melissa K. Gardner,[1,2,3] Blake D. Charlebois,[4] Imre M. Jánosi,[5] Jonathon Howard,[2] Alan J. Hunt,[4,*] and David J. Odde[1,*]
[1]Department of Biomedical Engineering, University of Minnesota, Minneapolis, MN 55455, USA
[2]Max Planck Institute of Molecular Cell Biology and Genetics, Dresden, Germany
[3]Department of Genetics, Cell Biology, and Development, University of Minnesota, Minneapolis, MN 55455, USA
[4]Department of Biomedical Engineering, University of Michigan, Ann Arbor, MI 48109, USA
[5]Department of Physics of Complex Systems, Loránd Eötvös University, Budapest, Hungary
*Correspondence: ajhunt@umich.edu (A.J.H.), oddex002@umn.edu (D.J.O.)
DOI 10.1016/j.cell.2011.06.053

SUMMARY

Microtubule assembly is vital for many fundamental cellular processes. Current models for microtubule assembly kinetics assume that the subunit dissociation rate from a microtubule tip is independent of free subunit concentration. Total-Internal-Reflection-Fluorescence (TIRF) microscopy experiments and data from a laser tweezers assay that measures in vitro microtubule assembly with nanometer resolution, provides evidence that the subunit dissociation rate from a microtubule tip increases as the free subunit concentration increases. These data are consistent with a two-dimensional model for microtubule assembly, and are explained by a shift in microtubule tip structure from a relatively blunt shape at low free concentrations to relatively tapered at high free concentrations. We find that because both the association and the dissociation rates increase at higher free subunit concentrations, the kinetics of microtubule assembly are an order-of-magnitude higher than currently estimated in the literature.

INTRODUCTION

Microtubules are rapidly adaptable multi-stranded linear polymers that self-assemble and function in many crucial cellular processes such as cell division, intracellular transport, cell polarization, and nerve regeneration. To produce the length changes required during these cellular processes, microtubule ends stochastically switch between growing and shortening phases (Mitchison and Kirschner, 1984). Microtubules are most frequently observed as a column of thirteen protofilaments, each consisting of αβ-tubulin subunits stacked end-to-end. Thus, microtubules grow and shorten at their ends via the addition and loss of αβ-tubulin subunits from the individual protofilaments, and are stabilized by the combination of lateral and longitudinal bonds between subunits.

Microtubule assembly kinetics are important during cellular morphogenesis and are a target of widely used medical treatments. As a result, they have been the subject of intensive analysis for over three decades (Desai and Mitchison, 1997). Microtubule assembly is altered by drugs used to treat diseases such as cancer, gout, and artery restenosis. In addition, in vivo microtubule assembly dynamics are regulated by microtubule-associated proteins (MAPs), which act to alter tubulin subunit addition and/or loss rates (Howard and Hyman, 2007).

The tubulin subunit association and dissociation rate constants, $k_{on,MT}$ (μM^{-1} s^{-1}) and $k_{off,MT}$ (s^{-1}), respectively, have been previously estimated from in vitro measurements of the net microtubule assembly rate, v_g (subunits/s; with ~1625 subunits/μm of MT length), as a function of the free-tubulin concentration [Tub] (μM) (Table S1). These rate constants have been estimated by fitting the microtubule assembly data to a linear one-dimensional (1D) model, initially applied to biological polymers by Oosawa (1970). A key, but untested, assumption in the 1D model is that the tubulin subunit dissociation rate is constant regardless of free-tubulin concentration. This assumption cannot be strictly correct since it requires that the microtubule tip structure is on average constant over varying tubulin concentrations, which is not thermodynamically tenable (Hill, 1986). In addition, microtubule tips shift from relatively blunt tip structures at low tubulin concentration to relatively tapered tip structures at high concentrations (Chretien et al., 1995). However, the 1D model might still serve as a reasonable approximation if the microtubule tip structure is only weakly dependent on free-tubulin subunit concentration. Thus, the canonical view of microtubule polymerization implicitly rests on the assumption that all tubulin subunits at the tip of a growing microtubule are on average energetically similar to one another, so that $k_{off,MT}$ is independent of free subunit concentration.

To explicitly test whether thermodynamic differences between tubulin subunits at the microtubule tip are important for interpreting growth data, we used total internal reflection fluorescence (TIRF) microscopy, and our high temporal and spatial resolution nanoscale laser tweezer assay (Schek et al., 2007) to study microtubule assembly at near-molecular resolution. We show (1) that tubulin subunit dissociation rates from the tip of a growing microtubule depend on the free-tubulin concentration, and (2) that dissociation rates increase substantially at higher free-tubulin concentrations, which requires that the tubulin subunit on-off kinetics during microtubule growth occur 10× more rapidly than previously appreciated. Together, these data lead to a new perspective on the regulation of microtubule assembly via MAPs and drugs, where weak and infrequent interactions with tubulin subunits at the growing microtubule tip can strongly affect net assembly.

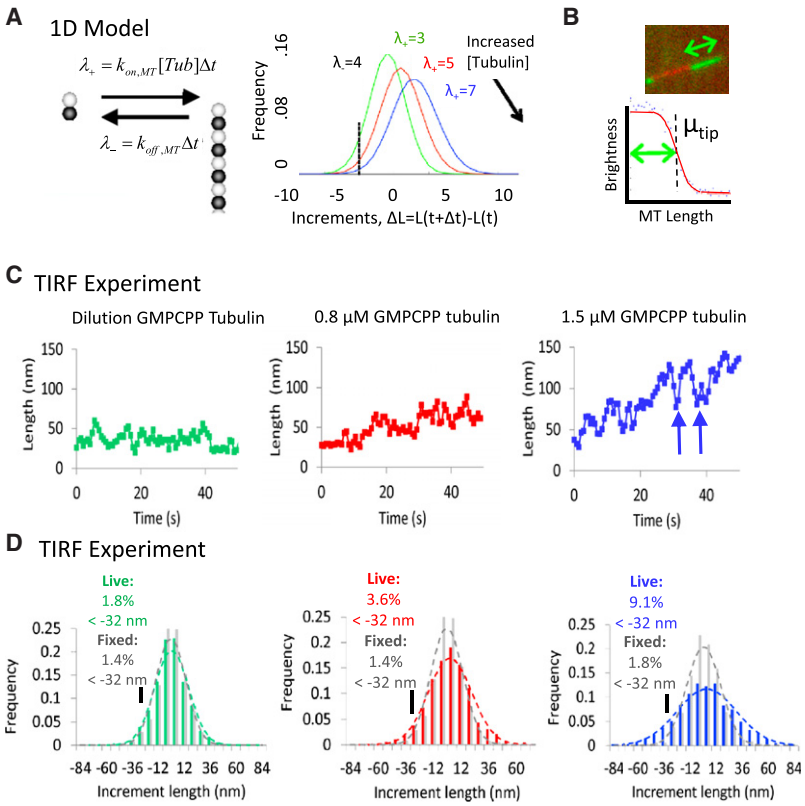

Figure 1. Direct Observation of Microtubule Assembly via TIRF Microscopy Reveals that the Tubulin Off Rate Increases at Higher Free-Tubulin Concentrations

(A) Elements of a "1D" model, initially described by Oosawa (1970) (left). Here, the number of tubulin subunits added to the microtubule tip (λ_+) in a time interval Δt increases proportionately to the tubulin concentration, while the number of subunits lost from the tip (λ_-) remains constant regardless of the free-tubulin concentration. Thus, large shortening events should decrease in frequency as the tubulin concentration is increased (i.e., as λ_+ increases). Given the number of arrivals, λ_+, and the number of departures, λ_-, the resulting difference, (λ_+-λ_-), gives the distribution of incremental microtubule length changes (right). An untested prediction of the 1D model is that the likelihood of large microtubule shortening events will decrease as the subunit arrival rate (λ_+) becomes larger. Therefore, the probability of a large shortening event (see dashed vertical line located at $|\lambda_+-\lambda_-| = |-4|$ at right) decreases with increasing free-tubulin concentration.

(B) Microtubule length measured using TIRF microscopy. Microtubule extensions (green), grown from GMPCPP microtubule seeds (red), are visualized during growth at varying GMPCPP-Tubulin concentrations. Tip position (μ_{tip}) is measured by fitting the decay in fluorescence intensity to the error function.

(C) Typical microtubule growth traces at different free concentrations of GMPCPP-Tubulin. Growth rate variability appears higher at 1.5 μM GMPCPP-Tubulin (right) as compared to a dilution experiment (left), and the magnitude of shortening events increases at higher tubulin concentrations (blue arrows).

(D) Quantification of growth rate variability. Length increments over 1.4 s intervals are summarized for each concentration. The fixed microtubule increment distribution (gray dashed line) is narrower than the live increment distribution for both 0.8 and 1.5 μM ($p = 0.018$ and $p = 0.002$ by t test, respectively), and large negative (shortening) increments are more common at higher GMPCPP-tubulin concentrations. For example, shortening events that are less than −32 nm account for 1.8% of all length increments in the dilution experiments, while length increments that are less than −32 nm are 9.1% of all increments at a GMPCPP-tubulin concentration of 1.5 μM. The fraction of length change increments for *fixed* microtubules remains relatively unchanged (1.4% at a pre-fix tubulin concentration of 0.6 μM, and 1.8% at a pre-fix concentration of 1.5 μM).

RESULTS

The 1D Model Predicts Fewer Large Shortening Events at Higher Tubulin Concentrations

In a linear (1D) model, a key assumption is that the departure rate of tubulin subunits from the microtubule tip ($k_{off,MT}$) is constant regardless of the free-tubulin concentration (Oosawa, 1970). As shown in Figure 1A (left), this model can be characterized by the number of tubulin subunit arrivals to the microtubule tip (λ_+) in a time interval Δt, which is determined by the on rate constant ($k_{on,MT}$) and the free-tubulin concentration ([Tub]). In this model, the number of departure events from the tip (λ_-) in a time interval Δt depends only on a fixed off rate constant ($k_{off,MT}$), and thus remains constant regardless of the free-tubulin concentration.

Given the number of arrivals, λ_+, and the number of departures, λ_-, the resulting difference, (λ_+-λ_-), gives the distribution of incremental microtubule length changes (Figure 1A, right). An untested prediction of the 1D model is that the likelihood of large microtubule shortening events will *decrease* as the subunit arrival rate (λ_+) becomes larger (Figure 1A, right). This is because microtubule growth is favored when the rate of subunit departure remains constant and the rate of subunit arrival increases in the presence of increasing [Tub]. Therefore, the probability of a large shortening event (see dashed vertical line located at $|\lambda_+-\lambda_-| = |-4|$) decreases with increasing free-tubulin concentration (Figure 1A, right). To directly test this prediction of the 1D model, we quantified the distribution of microtubule length increments as a function of free-tubulin concentration, asking if the frequency of large shortening events does in fact *decrease* at higher tubulin concentrations.

Microtubule Shortening Events Increase at Higher Tubulin Concentrations in TIRF Experiments

To test the 1D model predictions, we performed in vitro GMPCPP-tubulin experiments to measure microtubule assembly dynamics at nanometer scale resolution. Using GMPCPP allowed us to focus on the intrinsic variability in the microtubule growth rate without the potentially confounding effects of nucleotide hydrolysis. Assembly of GMPCPP-tubulin labeled with Alexa-488 (55% labeled, Invitrogen Corp.) onto Rhodamine-labeled GMPCPP-tubulin seeds was imaged by TIRF

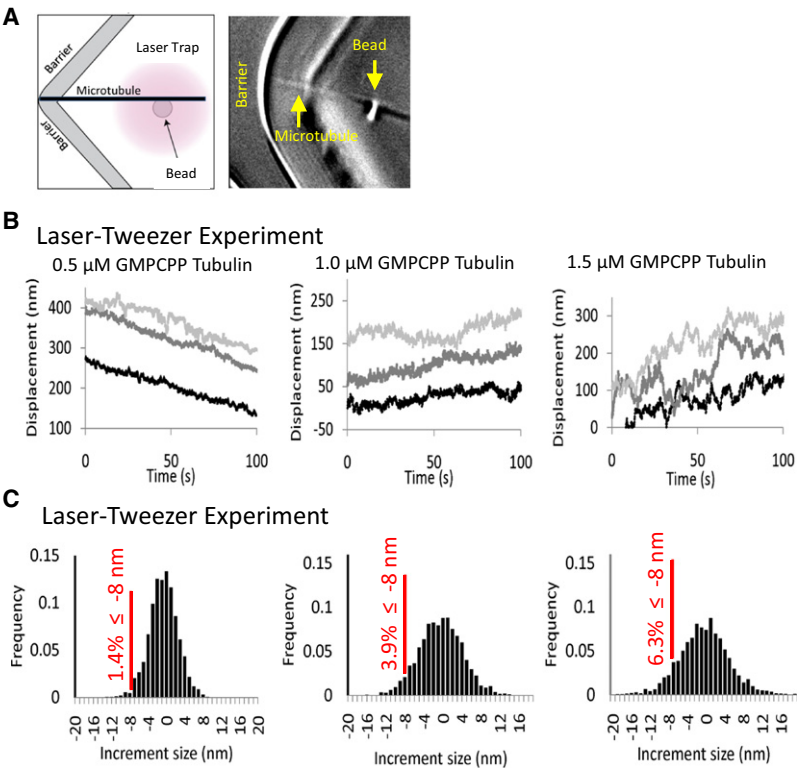

Figure 2. Nanoscale Optical Tweezers Experiments Confirm Increasing Growth Rate Variability and Frequency of Large Shortening Events at Higher Tubulin Concentrations

(A) In laser tweezer experiments, the position of a microtubule-attached bead is monitored as the microtubule tip grows against a microfabricated barrier.

(B) Net assembly rate variability is measured with increasing free GMPCPP-tubulin concentrations. The microtubule growth rate variability becomes larger (i.e., noisier) with increasing free-tubulin concentration.

(C) Histograms of microtubule length change increments at 0.1 s intervals show increased variability with increasing tubulin concentration, and large microtubule shortening events increase in frequency at higher free-tubulin concentrations (percentages of increments that are ≤ -8 nm shown in red), consistent with the TIRF measurements.

microscopy (Figure 1B). The positions of microtubule ends were estimated by fitting the error function to the fluorescence intensity at microtubule end, where the microtubule end was defined as the position at which the error function fell to 50% of the signal (μ_{tip}, Figure 1B) (Demchouk et al., 2011).

As expected, the rate of net assembly increased as the GMPCPP-tubulin concentration increased (Figure 1C). We found that microtubule growth trajectories in dilution experiments and at 0.8 μM GMPCPP-tubulin (Figure 1C, green and red, respectively) showed steady growth or shortening with small length fluctuations, while microtubule growth trajectories at 1.5 μM GMPCPP-tubulin (Figure 1C, blue) appeared to grow "noisily" with larger length fluctuations. These fluctuations were quantified by calculating the net length change increments for each 1.4 s interval during the first 30 s of growth for each microtubule (Figure 1D).

Using the TIRF system, we found that the frequency of large shortening events (e.g., < −32 nm, equivalent to 4 dimer lengths) increases at higher tubulin concentrations (from 1.8 ± 0.4% in dilution experiments to 9.1 ± 0.8% at 1.5 μM tubulin, Figure 1D). We note that for fixed (non-dynamic) microtubules the frequency of "shortening" events arising from measurement noise alone is approximately independent of tubulin concentration, ranging from 1.4 ± 0.4% at low concentration to 1.8 ± 0.4% at high concentration. Thus, the increase in the frequency and magnitude of shortening events at higher tubulin concentrations strongly suggests that the tubulin subunit dissociation rate from the microtubule tip increases at higher free-tubulin concentrations, which invalidates a basic assumption of the 1D model.

Microtubule Shortening Events Increase at Higher Tubulin Concentrations in Laser Tweezers Experiments

To examine microtubule growth rates with higher resolution, we measured the variability in growth rates using a nanoscale laser tweezers assay (Charlebois et al., 2010; Schek et al., 2007), which achieves a spatial resolution of < 3.5 nm at 10 Hz temporal resolution by measuring the position of microtubule-attached beads as microtubules grow into a microfabricated barrier (Figure 2A). We observed variability in microtubule growth at three different GMPCPP-tubulin concentrations, with variability increasing substantially at higher tubulin concentrations (Figure 2B). By quantitatively comparing the growth increment sizes at 0.1 s time intervals, we found that the frequency of large shortening events (e.g., < −8 nm) increased from 1.4 ± 0.3% of all events at 0.5 μM tubulin, to 6.3 ± 0.5% of all events at 1.5 μM tubulin (Figure 2C). Because of the higher spatial-temporal resolution in the tweezers experiment, we tested for the addition of oligomers (Kerssemakers et al., 2006; Schek et al., 2007). We never observed increments equal to or larger than 16 nm (i.e., two subunits) at 0.5 μM and 1.0 μM (n = 4998 increments), and only rarely at 1.5 μM (0.93%, n = 2567 increments). These rare instances of additions larger than 16 nm could be explained by rapid successive addition events of single subunits (Schek et al., 2007). Thus, similar to the TIRF data, the optical tweezers data indicates that the tubulin subunit dissociation rate from the microtubule tip increases at higher tubulin concentrations, which is inconsistent with the 1D model.

Lateral and Longitudinal Bonds Influence the Concentration-Dependent Subunit Dissociation Rates

Because the tubulin dissociation rate from the microtubule tip increases at higher tubulin concentrations, we asked if the state of the microtubule tip is on average shifted to a less stable configuration at higher tubulin concentrations. To ask this question, we performed computer simulations using our previously published "2D" model for microtubule assembly (VanBuren et al., 2002). In contrast to the 1D model, where protofilaments

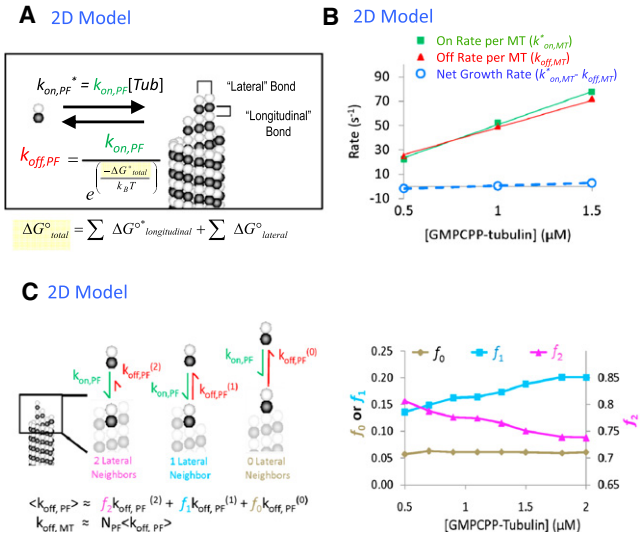

Figure 3. A 2D Model Predicts that Tubulin Subunit Dissociation Rates Are Dependent on Free Subunit Concentration

(A) Microtubules grow and shorten via the addition and loss of αβ-tubulin subunits. A 2D model includes the effect of both lateral bond interactions between neighboring protofilaments and longitudinal bonds along the protofilament.

(B) The 2D model predicts that tubulin dissociation rates increase at higher tubulin concentrations (red). Thus, the net assembly rate (blue) is given by the small difference between the large on rate (green) and the large off rate (red).

(C) Left: Dissociation rates at growing microtubule tips vary for each protofilament based on the number of lateral neighbor interactions at the protofilament tip. Here, dissociation rates are high for tubulin subunits with fewer lateral neighbors, while more lateral neighbors results in reduced dissociation rates. Right: The 2D model predicts that 1-neighbor protofilament tip interactions increase in likelihood at higher free subunit concentrations, while 2-neighbor interactions decrease with increasing free subunit concentration.

are regarded as independent with a single $k_{off,PF}$, the 2D model explicitly accounts for the bonds in both the lateral and longitudinal directions. Together, these bonds stabilize a subunit. As the number of these bonds varies, $k_{off,PF}$ will also change. Since the number of lateral bonds between subunits at the tip depends on the tip structure, $k_{off,PF}$ averaged over time and all protofilaments yields $k_{off,MT}$. This value for $k_{off,MT}$ could increase at higher tubulin concentrations, consistent with our experimental observations (Figures 1 and 2). Therefore, we asked whether the 2D model predicts an increase in $k_{off,MT}$ at higher tubulin concentrations.

The 2D simulation accounts for (1) subunit arrivals at the tip of the microtubule, and (2) subunit departures from the tip (Figure 3A). For arrivals, the subunit arrival rate at the tip of a protofilament ($k_{on,PF}^*$) is given by:

$$k_{on,PF}^* = k_{on,PF}[Tub] \quad (1)$$

where $k_{on,PF}$ is the on rate constant per individual protofilament ($\mu M^{-1}s^{-1}$, such that $k_{on,MT} = 13^*k_{on,PF}$), $k_{on,PF}^*$ is the arrival rate per individual protofilament (s^{-1}, similarly $k_{on,MT}^* = 13^*k_{on,PF}^*$), and [Tub] is the free-tubulin subunit concentration. This expression for tubulin subunit arrival rate to each protofilament is identical to the 1D model. However, to account for energetic differences between tubulin subunits at the microtubule tip, in the 2D model the subunit departure rate from a given protofilament, $k_{off,PF}$, depends on the equilibrium constant, where

$$K_{eq} \equiv \frac{k_{on,PF}}{k_{off,PF}} = e^{-\Delta G^0_{total}/k_BT} \quad (2)$$

Therefore, by rearrangement:

$$k_{off,PF} = \frac{k_{on,PF}}{e^{-\Delta G^0_{total}/k_BT}} \quad (3)$$

where $k_{off,PF}$ is the off rate per individual protofilament (s^{-1}), k_B is Boltzmann's constant, T is absolute temperature, and ΔG^0_{total} is the total free energy of the stabilizing bonds on a specific subunit, given by

$$\Delta G^0_{total} = \sum \Delta G^{0*}_{Longitudinal} + \sum \Delta G^0_{Lateral} \quad (4)$$

Tip subunits will (by definition) have one longitudinal bond (Figure 3A), and therefore the total value for $\Delta G^{0*}_{Longitudinal}$ will be identical for all subunits at the tip. However, the *lateral* bond energy ($\Delta G^0_{Lateral}$) will vary, such that subunits with two lateral neighbors will have a two-fold more negative value for $\Delta G^0_{Lateral}$ than subunits with only one lateral neighbor.

As the stochastic 2D model computer simulation proceeds (see animated Movie S1 and Movie S2), the tip structure evolves as subunits arrive and depart from the tip of each protofilament, and the average behavior can be calculated for a given tubulin concentration (simulation parameters in Table S2 and Figure S1). The steady-state subunit off rate from the microtubule tip (averaged over time and summed over all protofilaments) can then be calculated as a function of the free subunit concentration. The 2D model predicts that net microtubule assembly (Figure 3B, blue) results from the relatively small difference between a large subunit arrival rate that increases with free-tubulin concentration (Figure 3B, green), and a large subunit departure rate that *also* increases with increasing free-tubulin concentration (Figure 3B, red). Thus, the 2D model assumes that subunits at the tip of a growing microtubule are not energetically identical, and therefore predicts that the average $k_{off,MT}$ increases at higher tubulin concentrations. This result provides an explanation for the discrepancy between our experimental observations and the 1D model.

Why do the subunit dissociation rates increase at higher free-tubulin concentrations? The protofilament dissociation rate constant is dependent on the number of neighboring protofilaments available for forming stabilizing lateral bonds (Figure 3C), which must on average be shifted toward less stable configurations as the tubulin concentration increases. For example, tubulin subunits with two lateral neighbors (Figure 3C, left) have a low dissociation rate constant, while subunits with one lateral neighbor have a moderate dissociation rate constant, and tubulin subunits with no lateral neighbors have a high dissociation rate constant due to the lack of any stabilizing lateral bonds (Figure 3C, left). Thus, if the probability of the configurations was known, the dissociation rate constant averaged over the entire microtubule tip ($k_{off,MT}$) would be given by

$$k_{off,MT} \approx f_2 k_{off,PF}^{(2)} + f_1 k_{off,PF}^{(1)} + f_0 k_{off,PF}^{(0)} \quad (5)$$

where f_2, f_1, and f_0 are the mean probabilities of tubulin subunits at the tip with two, one, and zero lateral neighbors, respectively, and $k_{off,PF}^{(2)}$, $k_{off,PF}^{(1)}$, and $k_{off,PF}^{(0)}$ are the individual protofilament dissociation rate constants for a tubulin subunit with two, one, and zero lateral neighbors, respectively (Stukalin and Kolomeisky, 2004).

We examined how the relative fractions of tubulin subunits with 0, 1, or 2 lateral neighbors change with increasing free subunit concentrations in the 2D model and found that the fraction of tubulin subunits at microtubule tips with 0 lateral neighbors remains relatively constant at all concentrations (Figure 3C, right, yellow). However, there is an increase in the probability of relatively unstable 1 lateral neighbor subunits at the microtubule tip with increasing tubulin concentration (Figure 3C, right, blue), and a corresponding decrease in the probability of relatively stable tubulin subunits having 2 lateral neighbors (Figure 3C, right, magenta). Thus, the off rate is indirectly dependent upon the on rate. This is because the tip becomes more extended (i.e., protofilament lengths are more variable with increasing tendency toward only one lateral neighbor) as the on rate increases, which in turn increases the off rate. Thus, the off and on rates rise together.

The 1D and 2D Models Predict Different Kinetic Rate Constants for Microtubule Assembly

Numerous in vitro studies have confirmed the predicted linear relationship between growth velocity and free concentration for growing GTP-tubulin microtubules and for GMPCPP-tubulin microtubules. These studies, summarized in Table S1, have consistently yielded average association rate constants $k_{on,MT}$ of $\approx$5 μM^{-1} s^{-1} (range 1–9 μM^{-1} s^{-1}) and average dissociation rates of $k_{off,MT} \approx 15$ s^{-1} (range 0.1–44 s^{-1}).

Similar to these studies, we experimentally measured the microtubule growth velocity as a function of GMPCPP-tubulin concentration using both the in vitro TIRF and the nanoscale laser tweezers assays. We then calculated the 1D model association and dissociation rate constants using the combined results from both experiments (Figure 4A). From the slope and intercept, the 1D model microtubule association rate constant for GMPCPP-Tubulin was $k_{on,MT} = 5.1$ $\mu M^{-1} s^{-1}$, and the dissociation rate constant was $k_{off,MT} = 3.9$ s^{-1}. Thus, our observed growth velocity dependence on tubulin concentration was within the range previously observed and yields similar 1D model rate constants to those previously reported (Table S1).

The 2D model also predicts a linear relationship between microtubule growth velocity and tubulin concentration (Figure 4B). However, the 2D model predicts that the average dissociation rate increases approximately linearly with free-tubulin concentration due to evolving tip structures (Figure 3B). This in turn requires that the association rate constant is substantially larger than in a 1D model in order to produce the observed net microtubule growth rate (Figure 3B and Figure 4B). As a result, the 2D model association rate constant must be approximately an *order of magnitude* higher than the association rate constant estimated for the 1D model ($k_{on,MT} \approx 52$ $\mu M^{-1} s^{-1}$ with a 2D model, see Figure S1 and Table S2) (Figure 4B). This 2D model association rate constant, when considered on a per protofilament basis ($k_{on,PF} = k_{on,MT}$ /13 = 4 μM^{-1} s^{-1}), is consistent with theoretical predictions for rotational-translational diffusion-limited protein-protein association reactions (Northrup and Erickson, 1992) and is similar to that estimated for F-actin (2 protofilament) self-assembly on a per protofilament basis, $k_{on,filament} = 11.6$ $\mu M^{-1} s^{-1}$ or $k_{on,PF} = 5.8$ $\mu M^{-1} s^{-1}$ (Pollard, 1986).

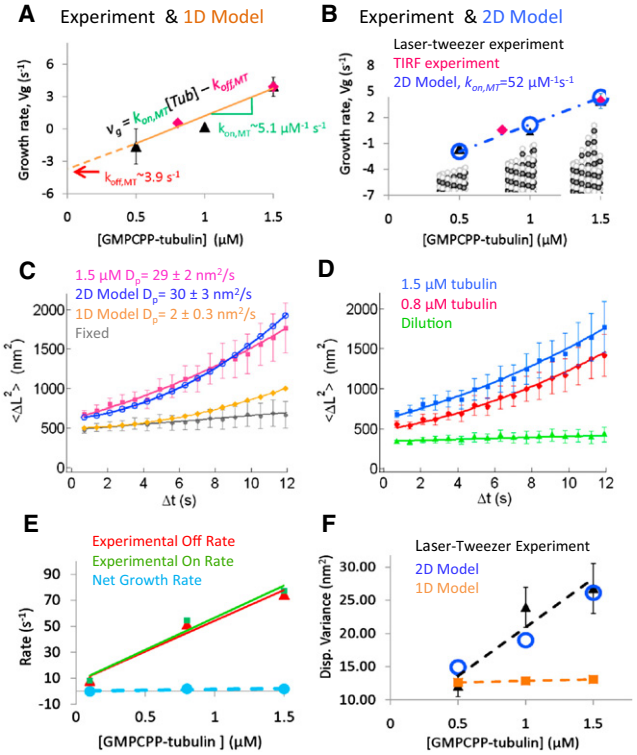

Figure 4. Lateral Neighbor Interactions Require Rapid On-Off Kinetics for Tubulin Subunits at the Microtubule Tip

(A) The 1D model of Oosawa (1970) was used to estimate αβ-tubulin association and dissociation rate constants for GMPCPP-tubulin microtubules.

(B) Similar to the 1D model, a 2D model also predicts a linear microtubule growth rate increase with increasing concentration, but with a rate constant that is an order of magnitude higher than in the 1D model.

(C) A 2D model with rapid kinetics predicts experimental microtubule growth variability in the TIRF assay, whereas a 1D model with low subunit association and dissociation rates fails to reproduce the experimentally observed microtubule growth rate variability.

(D) By analyzing the mean-squared displacement versus time-step data at different tubulin concentrations, the tubulin subunit on rates, off rates, and net rates can be estimated in each case, as summarized in Table S3 and (E).

(E) Experimental tubulin subunit on rates and off rates as a function of GMPCPP-tubulin concentration. Similar to the 2D model prediction (Figure 3B), the tubulin dissociation rate rises with increasing tubulin concentration (red). The net assembly rate (blue) is given by the small difference between the large on rate (green) and the large off rate (red).

(F) A 2D model with rapid assembly kinetics predicts experimental microtubule growth variability in the GMPCPP-tubulin nanoscale laser-tweezer assay, while a 1D model with slow kinetics fails to reproduce the experimentally observed microtubule growth rate variance at higher GMPCPP-tubulin concentrations.

The Rapid On-Off Kinetics Required in the 2D Model Accurately Predict the Variability in Growth Rate

For a stochastic process the variance in the number of events per time interval is equal to the mean number of events. Therefore the variability in microtubule growth rate should reflect the underlying rates of subunit addition and loss. Since the 2D model predicts rate constants that are an order of magnitude higher than the 1D model, it also predicts a much larger variance in the microtubule assembly rate. To quantitatively compare the predictions of the 1D and 2D models to our experimental results, we calculated the mean squared displacement of microtubule length increments for increasing time steps, and plotted the results for each model with the 1.5 μM TIRF experimental data (Figure 4C). By plotting the results in this manner, the length fluctuations of filament growth can be described by a diffusion with drift equation, as given by:

$$\langle \Delta L^2 \rangle = v_g^2 \Delta t^2 + 2D_p \Delta t + \sigma^2 \quad (6)$$

where ΔL is the microtubule length change increment (in nm) over a given time step Δt (in sec), v_g is the net growth rate (nm/s), and D_p is the effective diffusion coefficient for the microtubule polymerization, which provides a quantitative measure of the variability in microtubule growth increments. Finally, σ^2 is the experimental measurement noise.

By fitting the experimental data and both models' predicted data to a quadratic equation, the diffusion coefficient (D_p) can be estimated, which provides a quantitative measure of the microtubule growth variability. The 1D model diffusion coefficient D_p (constrained by mean growth rate data to $k_{on,MT}$ = 5.1 μM^{-1} s^{-1} and $k_{off,MT}$ = 3.9 s^{-1}, as in Figure 4A) is an order of magnitude lower than the experimental diffusion coefficient (Figure 4C). In contrast, the 2D model, constrained by the mean growth rate experiments to a 10-fold higher association rate constant than in the 1D model ($k_{on,MT}$ = 52 μM^{-1} s^{-1}), predicts a diffusion coefficient D_p, that is similar to the experimental data (Figures 4C and 2D model parameters as in Table S2). Thus, microtubule assembly is too variable to be consistent with the 1D model, but is consistent with the 2D model.

Experiments Confirm Rapid Tubulin On-Off Kinetics as Predicted by the 2D Model

The tubulin subunit on rate ($k_{on,MT}$*) and the off rate ($k_{off,MT}$) from the microtubule tip can be directly estimated from the mean-squared displacement versus time data (Figure 4D). The diffusion coefficient, D_p, relates the microtubule length mean squared displacement due to diffusion alone, $\langle \Delta l_D^2 \rangle$, to the time interval, Δt, via

$$\langle \Delta l_D^2 \rangle = 2D_p \Delta t \quad (7)$$

and the growth rate variance due to diffusion is described by a Skellam distribution (Oosawa, 1970; Skellam, 1946), so that

$$\langle \Delta l_D^2 \rangle = a^2 (k_{on,MT}[Tub] + k_{off,MT}) \Delta t \quad (8)$$

where a is the change in microtubule length contributed by a single dimer, which is on average 0.615 nm. Combining Equations (7) and (8) and solving for D_p we obtain,

$$D_p = \frac{a^2}{2}(k_{on,MT}[Tub] + k_{off,MT}) \quad (9)$$

In addition, by definition,

$$v_g = a(k_{on,MT}[Tub] - k_{off,MT}) \quad (10)$$

Thus, through these two Equations (9) and (10), the two unknowns, $k_{on,MT}$ and $k_{off,MT}$, can be directly calculated at a given tubulin concentration using the experimentally estimated values of D_p and v_g.

To calculate the values for $k_{on,MT}$ and $k_{off,MT}$ from the experimental data, and to confirm concentration-dependent tubulin subunit dissociation rates, we completed the mean-squared displacement analysis as described above for a range of free-tubulin concentrations in the TIRF analysis (Figure 4D). Detailed results are summarized in Table S3 and shown in Figure 4E. The experimentally estimated tubulin dissociation rate increases substantially as the tubulin concentration is increased, and the relatively slow net experimental microtubule assembly rate (blue) represents the difference between a large experimental on rate (green) and a large off rate (red), similar to the 2D model prediction (Figure 3B). For example, at 1.5 μM, the net microtubule assembly rate (blue) represents the difference between a large on rate, $k_{on,MT}$[Tub] ≈77 s^{-1} (green), and a large off rate, $k_{off,MT}$ ≈75 s^{-1} (red). In addition, the dilution experimental results demonstrate that the off rate collapses to very near the 1D model estimate when microtubule tips are blunt (1D model $k_{off,MT}$ ≈4 s^{-1}, estimated experimental $k_{off,MT}$ in dilution experiment, ≈8 s^{-1}).

We then asked whether, consistent with the TIRF assays, the variance in the growth rate measured using the optical tweezers assay is quantitatively larger than expected for the 1D model. As shown in Figure 4F, the 1D model, constrained by mean growth rate data to $k_{on,MT}$ = 5.1 μM^{-1} s^{-1} and $k_{off,MT}$ = 3.9 s^{-1} (Figure 4A), predicts a microtubule growth rate variance in the laser tweezer assay of $\sigma^2_{Assembly}$ = 1.0 nm^2 at 0.5 μM tubulin ($k_{on,MT}$* = 2.5 s^{-1}) and $\sigma^2_{Assembly}$ = 1.7 nm^2 at 1.5 μM tubulin ($k_{on,MT}$* = 7.6 s^{-1}). Our laser tweezers assay has a measurement variance due to Brownian motion of the microtubule-bead complex of $\sigma^2_{Thermal}$ = (3.5 nm)^2 = 12 nm^2 (at 10 Hz) (Schek et al., 2007). Thus, the 1D model predicts that the experimentally observed variance, $\sigma^2_{Observed} = \sigma^2_{Assembly} + \sigma^2_{Thermal}$ = 1 nm^2 + 12 nm^2 = 13 nm^2, will be dominated by the thermal measurement noise and so will not depend on free subunit concentration (Figure 4F, orange line). Contrary to this expectation, the microtubule growth increment distribution from the laser-tweezer assay increases with the tubulin concentration, and is inconsistent with the 1D model at 1.0 μM ($p < 10^{-8}$, Two-tailed F-test) and 1.5 μM ($p < 10^{-8}$, Two-tailed F-test).

The 2D model, constrained by the mean growth rate experiments to a 10-fold higher association rate constant than the 1D model, predicts a substantial increase in growth rate variance with increasing tubulin concentration. For the 2D model at 0.1 s time intervals, the growth rate variance is predicted to increase from 15 nm^2 at 0.5 μM tubulin to 25 nm^2 at 1.5 μM tubulin (Figure 4F, blue, 2D model parameters as in Table S2) which is consistent with experimental results (1.0 μM, p = 0.47; 1.5 μM,

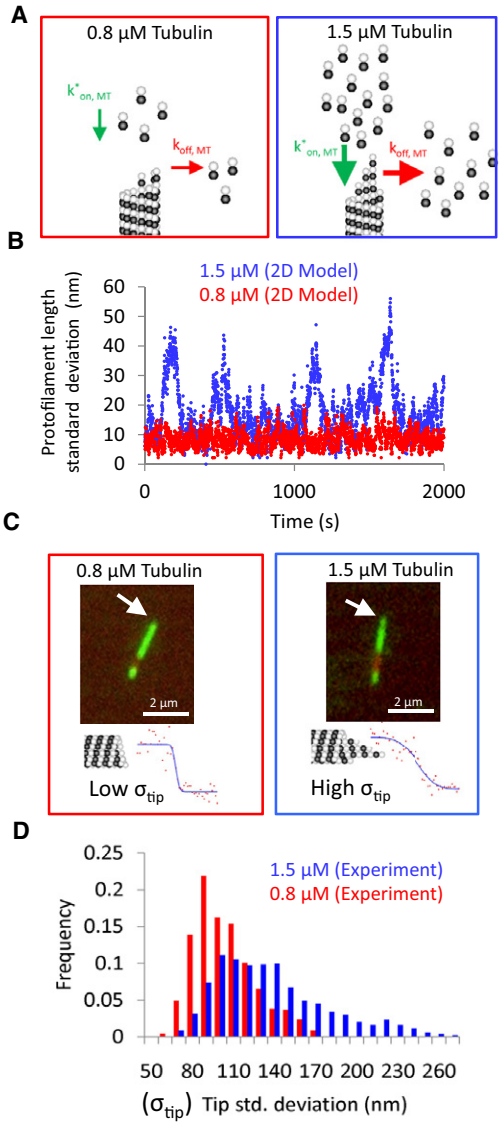

Figure 5. TIRF Microscopy Measurements Show that Microtubule Tip Structure Depends on Free GMPCPP-Tubulin Concentration

(A) A 2D model predicts that tip structures at higher free-tubulin concentrations will exhibit a greater disparity in protofilament length.

(B) The standard deviation of protofilament lengths for a given microtubule (σ_{tip}) provides a measure of the variability in protofilament lengths. The 2D model predicts that σ_{tip} will, on average, be large in 1.5 μM tubulin (blue) relative to 0.8 μM tubulin (red).

(C) By fitting the decay in fluorescence intensity at the microtubule end to an error function, the standard deviation (σ_{tip}) of the error function is estimated, which reflects the variability in protofilament lengths at the microtubule tip. A low σ_{tip} (left) suggests that microtubule tips are blunt, with low variation in protofilament length. Conversely, a high σ_{tip} (right) suggests that tips are extended, with a higher variation in protofilament length.

(D) In TIRF experiments, the tip standard deviation (σ_{tip}) increases with increasing free GMPCPP-tubulin concentration. The mean tip standard deviation, $\langle \sigma_{tip} \rangle$, at a concentration of 0.8 μM GMPCPP-tubulin is 99 ± 22 nm (mean ± SD; n = 700), while $\langle \sigma_{tip} \rangle$ at 1.5 μM GMPCPP-tubulin is 140 ± 55 nm (mean ± SD; n = 1120; $p < 10^{-15}$) for similar length microtubules at both concentrations. This experimental result shows that microtubule tips are relatively blunt with low protofilament length variation in 0.8 μM GMPCPP-Tubulin, while they are more extended, with a larger variation in protofilament lengths, at 1.5 μM.

p = 0.31; Two-tailed F-Test). Thus, the experimentally measured microtubule growth variance at higher GMPCPP-Tubulin concentrations is inconsistent with the relatively slow kinetics predicted by the 1D model, but is well described using a 10-fold higher tubulin association rate constant.

Experiments Confirm that Microtubule Tips Are More Tapered as Tubulin Concentrations Increase

In shifting from low tubulin concentration (i.e., favoring two lateral neighbors, Figure 3C) to high concentration (i.e., favoring one lateral neighbor, Figure 3C), the microtubule tip structure predicted from the 2D model shifts from being relatively blunt, where protofilaments are typically the same length, to a more tapered tip in which protofilament lengths are more variable (Figure 5A). This is because at high tubulin concentration (i.e., when subunits arrive rapidly to the tip), protofilaments will tend to grow independently of their neighbors, which results in tip subunits that are more likely to have only 1 lateral neighbor. Specifically, the tip structures at higher free-tubulin concentrations will exhibit greater disparity in protofilament length (i.e., higher protofilament length standard deviation), with more single-neighbor protofilament extensions (Figure 5B, blue). In contrast, at low tubulin concentrations, the relatively higher off rate will favor blunt ends (i.e., lower protofilament length standard deviation), where two lateral neighbors predominate (Figure 5B, red). These predictions are consistent with cryo-electron microscopy images of microtubules formed from GTP-tubulin, where the mean microtubule tip taper lengths increase with increasing GTP-tubulin concentration (Chretien et al., 1995).

To test this prediction for GMPCPP microtubules, we estimated tip structures using TIRF microscopy by fitting the error function to the green Alexa-488 fluorescence intensity at microtubule ends, which yields both the mean protofilament length (μ_{tip}) (Figure 1B) and the standard deviation of protofilament lengths (σ_{tip}) (Figure 5C) (Demchouk et al., 2011). Specifically, we expect that tips with a smaller σ_{tip} have relatively "blunt" tips (Figure 5C, left), while tips with a larger σ_{tip} have more tapered tips (Figure 5C, right). Using this approach, we quantified the distribution of tip standard deviations (σ_{tip}) for similar lengths of Alexa-488 microtubules grown at 0.8 μM and 1.5 μM GMPCPP-Tubulin (Figure 5D). We found that the mean tip standard deviation, $\langle \sigma_{tip} \rangle$, is 99 ± 22 nm (mean ± SD; n = 700) at a concentration of 0.8 μM GMPCPP-Tubulin, while $\langle \sigma_{tip} \rangle$ at 1.5 μM GMPCPP-Tubulin is 140 ± 55 nm (mean ± SD; n = 1120) (Figure 5D). This difference in $\langle \sigma_{tip} \rangle$ measurements ($p < 10^{-15}$) suggests that microtubule tips are relatively blunt (with low protofilament length variation) in 0.8 μM GMPCPP-Tubulin, while at 1.5 μM they are more extended, with a larger variation in protofilament lengths. These results are consistent with the prediction that a decrease in the mean number of subunit lateral neighbors at the microtubule tip causes the mean subunit dissociation rate to accelerate with increasing free-tubulin concentration.

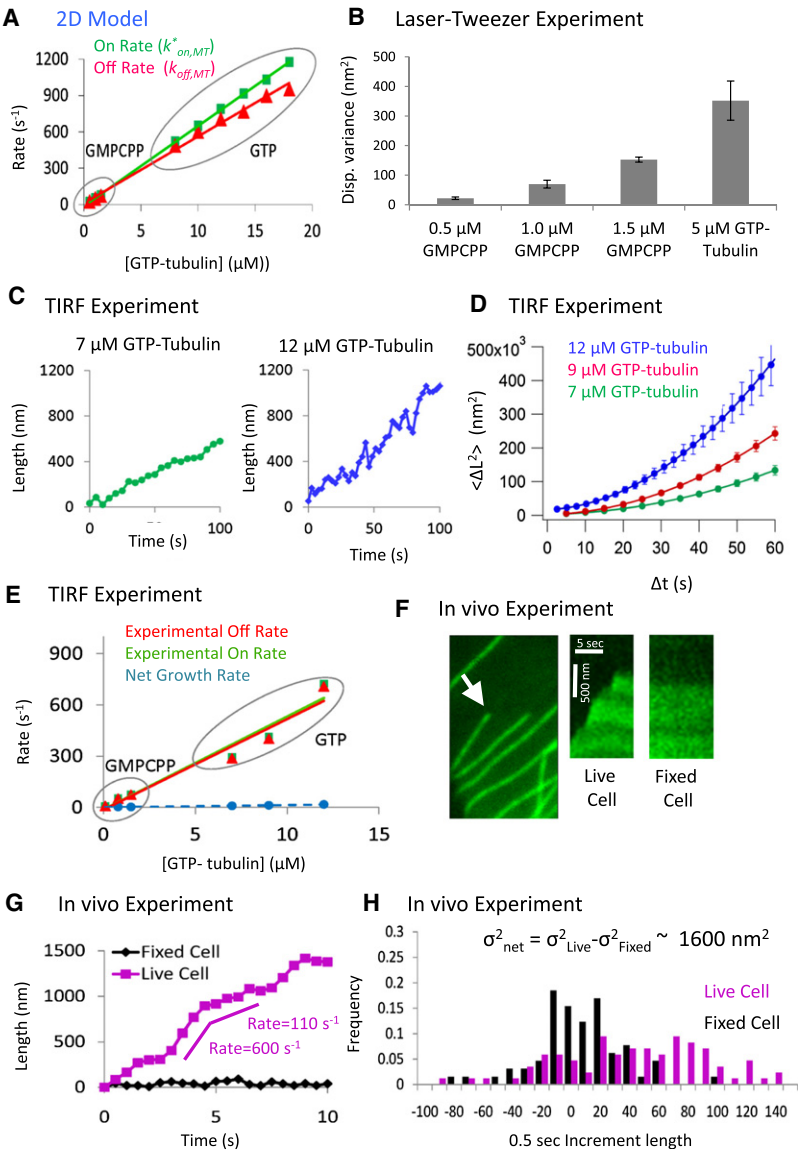

Figure 6. Physiological Tubulin Concentrations Result in Increased Growth Variability Both In Vitro and In Vivo

(A) A 2D model predicts that subunit association rates and subunit dissociation rates will continue to increase for GTP-tubulin at physiological free-tubulin concentrations.

(B) Because of rapid kinetics at higher free subunit concentrations, the microtubule growth rate variability continues to increase for higher GTP-tubulin concentrations (5 μM GTP-tubulin data from (Schek et al., 2007), downsampled to 0.5 s intervals).

(C) TIRF experiments with GTP-tubulin qualitatively show increasing growth variability at 12 μM tubulin as compared to 7 μM tubulin.

(D) By analyzing the mean-squared displacement versus time-step data at different GTP-tubulin concentrations, the tubulin subunit on rates, off rates, and net rates can be estimated in each case, as summarized in Table S3 and (E).

(E) Experimental tubulin subunit on rates and off rates are plotted as a function of GMPCPP-tubulin and GTP-tubulin concentration. Similar to the 2D model prediction (Figure 6A), the tubulin off rate rises with increasing tubulin concentration (red). The net assembly rate (blue) is given by the small difference between the large on rate (green) and the large off rate (red) (see also Table S3).

(F) Microtubule growth rates are measured near the cell periphery in both live and fixed LLC-PK1α cells to measure the variance in growth rate at 0.5 s intervals (green: GFP-tubulin).

(G) Microtubule length as a function of time for live and fixed microtubules. Growing microtubules frequently shift the net rate dramatically on a time scale of seconds. In this example, the net rate shifts from 600 s^{-1} to 110 s^{-1} in a period of a few seconds.

(H) In vivo microtubule growth rate variance is nearly 5-fold higher than GTP-tubulin in vitro data at 5 μM. In vivo growth rate variances are calculated by subtracting the fixed-cell measurement error variance from the live-cell data. Thus, the kinetic constants in vivo are at least as large as those estimated in vitro for GTP-tubulin at similar concentrations.

Rapid GTP-Tubulin On-Off Kinetics In Vitro at Physiological Concentrations

We then tested whether the conclusions from our GMPCPP tubulin experiments are consistent with GTP-tubulin experiments at physiological concentrations (Figure S2).

As is the case with GMPCPP-tubulin, the 2D model predicts that both $k_{on,MT}^*$ and $k_{off,MT}$ will increase at higher physiologic GTP-tubulin concentrations (Figure 6A). According to the 2D model, the increment variance will then increase proportionate to the tubulin concentration. Therefore, in our previous study with ~5 μM GTP-tubulin in an in vitro laser tweezers microtubule assembly assay (Schek et al., 2007) we should have observed a variance of ~3-fold larger than in our present 1.5 μM GMPCPP-tubulin experiments (5 μM/1.5 μM ~3). As shown in Figure 6B, the variance is ~3-fold higher at ~3-fold higher tubulin concentration (5 μM GTP-tubulin versus 1.5 μM GMPCPP tubulin both sampled at 0.5 s intervals).

We performed TIRF experiments with GTP-tubulin at 7, 9, and 12 μM, and we observed an increase in microtubule growth variability and in negative growth excursions in going from 7 μM tubulin to 12 μM tubulin (Figure 6C), similar to the GMPCPP tubulin data. As described above, we then fit the mean-squared-displacement data to the diffusion-drift model for each concentration (Figure 6D). Using this method, the tubulin subunit on rate ($k_{on,MT}^*$) and the off rate ($k_{off,MT}$) from the microtubule tip can be directly estimated from the data (Figure 6E, Table S3). Consistent with the GMPCPP tubulin experiments, the experimentally estimated tubulin dissociation rate increases substantially as the GTP-tubulin concentration is increased, and the net experimental microtubule assembly rate (blue) represents the small difference between a large experimental on rate (green) and a large off rate (red), similar to the 2D model prediction (Compare Figure 6A with Figure 6E).

The Kinetics of Microtubule Assembly

	Previously	This Study
$k_{on,MT}$	~5 $\mu M^{-1}s^{-1}$	~58 ± 4 $\mu M^{-1}s^{-1}$
$k_{off,MT}$	Constant	Concentration Dependent
Kinetics	Slow Kinetics 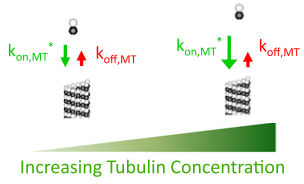	Rapid Tip-State Dependent Kinetics 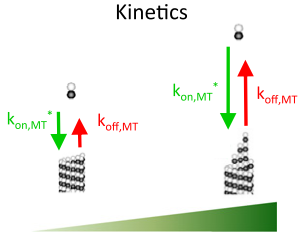

Figure 7. Revised View of Microtubule Assembly Kinetics

By accounting for a non-homogeneous tip structure in a 2D model of microtubule assembly, we find that (1) the association rate constant for tubulin subunits during microtubule assembly is an order of magnitude higher than previously thought, (2) the tubulin subunit dissociation rate is not constant, as previously assumed, but rather increases at higher tubulin concentrations, and (3) microtubule assembly is driven by rapid on and off events of individual tubulin subunits. Under typical assembly conditions, ~10 μM GTP-tubulin, the combined kinetic rates are estimated to occur at nearly 1000/s. At all tubulin concentrations the association and dissociation rates are nearly equal to each other.

In Vivo Microtubule Growth Variability Occurs with Rapid Tubulin Subunit On-Off Kinetics

To assess how our in vitro data compare with microtubule growth in vivo we measured microtubule growth at 0.5 s intervals near to the periphery of live LLC-PK1α cells, as previously described (Demchouk et al., 2011) (Figure 6F) (tubulin concentration estimate 5–15 μM, see Figure S2). To assess the measurement error, we also measured the length of microtubules in fixed LLC-PK1α cells at 0.5 s intervals. As shown in Figure 6G, there is high variability in live-cell microtubule growth rates, consistent with previous reports (Shelden and Wadsworth, 1993). With our high-resolution tracking accuracy (~36 nm) (Demchouk et al., 2011), we can now readily detect nanoscale changes in microtubule length, including periods where the growth rate abruptly shifts (Figure 6G). That the net rate is commonly ~600 s^{-1}, at least transiently, strongly suggests that the in vivo on-off dynamics are on the scale of 1 kHz. The in vivo variance in growth rate at 0.5 s intervals is ~1600 nm^2 (after subtracting the fixed microtubule variance), which is nearly 5-fold larger than the in vitro growth rate variance for GTP-tubulin microtubules at ~5 μM tubulin (Figure 6H, downsampled to 0.5 s intervals). Thus, the kinetic rate constants in vivo are at least as large as we estimate for in vitro assembly.

DISCUSSION

Implications for the Regulation of Microtubule Dynamics by MAPS and Drugs

The finding that tubulin association and dissociation rates are an order of magnitude higher than has been previously recognized, and nearly equal to each other at all concentrations, significantly changes the conceptualization of microtubule growth (Figure 7). Consequently, our thinking about regulation of assembly by MAPs and therapeutic drugs (such as taxol), also needs reassessment.

The near equality of on and off rates implies that infrequent and/or weak suppression of the off-rate should lead to dramatic shifts in net assembly for single microtubules in vivo (Figure 6G), and also implies that a slight tipping of the balance by a single MAP at the microtubule tip might significantly affect catastrophe and rescue in vivo. For example, weak suppression of the off rate by a stabilizing MAP would lead to a rapid and significant increase in the microtubule GTP-cap size, and a corresponding substantial decrease in catastrophe frequency. Furthermore, a much larger off rate allows a substantial range of growth regulation to be exerted purely through suppression of tubulin loss from the microtubule tip. This has important implications for explaining how a MAP such as XMAP215/chTOG, which is overexpressed in colon and hepatic tumors, promotes assembly. Growth rates in vivo, and with this MAP in vitro are commonly 2-10 fold higher than with pure tubulin at ~10 μM GTP-tubulin (Cassimeris et al., 1988; Charrasse et al., 1998; Pryer et al., 1992; Rusan et al., 2001; Shelden and Wadsworth, 1993; Vasquez et al., 1994). In the context of the 1D model, a 10-fold increase in growth rate can only be achieved by increasing the on rate because, for example, suppressing tubulin dissociation entirely (i.e., decreasing the off rate from 10 s^{-1} to 0 s^{-1}) would only achieve a 25% increase in net assembly rate. However, in the 2D model, a ten-fold increase in net growth rate by a MAP can be achieved simply by suppressing the off rate by a factor of two (see Figure S4). Such a mechanism of growth enhancement is similar to that proposed by Brouhard et al. (2008) and VanBuren et al. (2002) to account for the 5-fold acceleration of growth rate by XMAP215.

Conversely, even a weakly destabilizing MAP would be expected to tip the balance strongly toward catastrophe. The best understood catastrophe-promoting MAP, MCAK, seems to at least partly fulfill this description. The catalytic effect of MCAK at saturation is to increase the tubulin off-rate by 100-fold (Hunter et al., 2003), which in the 2D model corresponds to a modest free energy increase of $\Delta G^o = +\ln(100) = +4.6\ k_BT$. Interestingly, this energy turns out to be nearly equal in magnitude to our estimate of the lateral bond energy in the 2D model (−4.5-5.0 k_BT; Table S2). In addition, MCAK's catalytic effect on the off-rate is only weakly cooperative, so that even a single molecule is able to affect the off-rate (Hunter et al., 2003). The in vivo expression level of MCAK is crucial to maintenance of proper ploidy, which is important to avoid progression into a cancerous phenotype (Bakhoum et al., 2009a, 2009b).

An in vivo example of a weakly destabilizing MAP that tips the balance strongly toward catastrophe is the yeast kinesin-5 motor Cin8 (and to a lesser extent, Kip1; (Gardner et al., 2008)). During yeast mitosis, Cin8 promotes microtubule catastrophe in a length-dependent manner to mediate chromosome congression. Interestingly, the motor:microtubule ratio in vivo is very low, ~50 motors for ~40 microtubules in the yeast spindle, or nearly 1:1 overall (Gardner et al., 2008; Winey et al., 1995). Such a low ratio implies that the presence of even a single Cin8 motor at the plus end has a significant impact on the microtubule assembly state. From modeling studies, it was estimated that the presence of a single motor at the plus end was sufficient to promote catastrophe ~10-fold (Gardner et al., 2008). Given that metaphase yeast kinetochore microtubules contain on average about 600 tubulin dimers, the effect of the motor can be regarded as even more potent, with about one motor per ~600 tubulin dimers. Based on our present results, we suggest that such potency at low stoichiometry could be achieved with modest enhancement of the off rate, and/or suppression of the on rate, by one or a few motors.

Hypersensitivity of assembly can also potentially facilitate rapid cell-wide microtubule array reorganization. A prime example of a dramatic microtubule reorganization process is *Drosophila* embryo mitosis, where a mitotic spindle forms, segregates a genome, and subsequently disassembles in a matter of minutes (Stiffler et al., 1999). Such dramatic transitions in vivo occur under conditions of fixed total tubulin concentration, which serves to buffer perturbations to net assembly (Mitchison and Kirschner, 1987). For example, if an assembly-promoting MAP is upregulated, then the initial response will be potent. However, as net assembly is promoted, the free-tubulin concentration will drop, which will mitigate the assembly-promoting activity. Thus, constant total tubulin concentration will act to buffer and mitigate perturbations to microtubule dynamics, and confer a degree of robustness and homeostasis on the microtubule cytoskeleton. To overcome the built-in cell-level buffering effect and perform highly dynamic operations such as mitosis, the microtubule array needs to be hypersensitive.

To summarize, it will be important to revisit current models for microtubule regulation in vivo via MAPs and therapeutic drugs in light of our findings. In particular, because both on and off rates are rapid and nearly equal, MAPs that promote net microtubule assembly or disassembly could work through a modest changes in tubulin subunit kinetics (Brouhard et al., 2008; Murphy et al., 1977; Pryer et al., 1992; VanBuren et al., 2005, 2002).

Implications for Other Multistranded Filaments

More generally, our results identify a fundamental theoretical limitation to the 1D model of Oosawa, which has been used for nearly 40 years to interpret kinetic self-assembly data of microtubules, F-actin, viruses, and amyloid aggregates (Cannon et al., 2004; Collins et al., 2004). It will be important to revisit earlier 1D model-based studies to confirm that the assumption of constant subunit dissociation rates holds for self-assembled polymers containing both longitudinal and lateral interactions, since presently established kinetic estimates for these biological assemblies may need to be revised as we have found with microtubules.

EXPERIMENTAL PROCEDURES

Laser-Tweezer Experiments

Experimental observation of microtubule length changes at high spatial and temporal resolution were performed as described previously (Schek et al., 2007). Briefly, a microtubule linked to a 0.57 μm diameter silica bead was trapped by optical tweezers and oriented toward a microfabricated barrier. A weak force clamp was applied (~0.2 pN). Despite the applied force, thermal forces drive the microtubule tip away from the barrier, creating space for tubulin addition.

TIRF Experiments

Assembly of GMPCPP-Tubulin labeled with Alexa-488 (55% labeled, Invitrogen Corp.) onto Rhodamine-labeled GMPCPP-Tubulin seeds was imaged by TIRF microscopy as previously described (Gell et al.). Images were collected with an Andor iXon camera on a Zeiss Axiovert 200 M microscope using a Zeiss100X/1.45 NA Plan FLUAR objective. The Imaging Buffer consisted of BRB80 supplemented with 40 mM glucose, 40 mg/ml glucose-oxidase, 16 mg/ml catalase, 0.1 mg/ml casein and 1% β mercaptoethanol. A 2.5X Optovar was used to provide additional magnification and to limit pixel size to ~64 nm. An objective heater was used to warm the flow channel to 34°C for GMPCPP experiments. Although the time-lapse interval for collecting images was 700 ms, all images were collected at 100 ms exposure times, regardless of concentration. GTP-tubulin experiments were performed using 1 mM GTP to replace the GMPCPP.

Microtubule length and tip standard deviations were calculated as described previously (Demchouk et al., 2011). Similar length microtubules (2-3 μm) were used for our analysis regardless of concentration.

Dilution experiments were performed by allowing assembly of GMPCPP-Tubulin labeled with Alexa-488 (55% labeled, Invitrogen Corp.) from Rhodamine-labeled GMPCPP-Tubulin seeds until green microtubule extensions grew to 2-3 μm long, after which the free GMPCPP-Tubulin was flushed from the flow chamber 3 times using BRB80 supplemented with anti-fade reaction mixture. Depolymerization was observed.

Fixation experiments were performed by flowing in a mixture of BRB80 with 0.05% Glutaraldehyde once microtubule extensions achieved the appropriate length. Similar tip structure distributions were used for each concentration to accurately compare fixed and live microtubule growth increments. To account for potential microtubule tip tracking accuracy changes as a function of microtubule tip structure, we fixed microtubules after having grown them in the correct corresponding tubulin concentration in each case.

For expanded experimental details and information regarding calculations associated with the 1D and 2D models, please see Extended Experimental Procedures.

SUPPLEMENTAL INFORMATION

Supplemental Information includes Extended Experimental Procedures, four figures, three tables, and two movies and can be found with this article online at doi:10.1016/j.cell.2011.06.053.

ACKNOWLEDGMENTS

The authors thank Dominique Seetapun and Dr. Chris Gell for technical assistance. We thank Aleksey Demchouk for providing the microtubule tip tracking code. The LLC-PK1α strain was kindly provided by Dr. Pat Wadsworth. This work was supported by National Institutes of Health (NIH) GM076177 to A.J.H. and D.J.O, NIH GM071522 to D.J.O, and National Science Foundation (NSF) 615568 to D.J.O. M.K.G. was supported in part by a Whitaker International Scholar Fellowship. The collaboration was supported by the Institute for Mathematics and Its Applications (IMA) at the University of Minnesota.

Received: November 20, 2010
Revised: May 26, 2011
Accepted: June 30, 2011
Published: August 18, 2011

REFERENCES

Bakhoum, S.F., Genovese, G., and Compton, D.A. (2009a). Deviant kinetochore microtubule dynamics underlie chromosomal instability. Curr. Biol. *19*, 1937–1942.

Bakhoum, S.F., Thompson, S.L., Manning, A.L., and Compton, D.A. (2009b). Genome stability is ensured by temporal control of kinetochore-microtubule dynamics. Nat. Cell Biol. *11*, 27–35.

Brouhard, G.J., Stear, J.H., Noetzel, T.L., Al-Bassam, J., Kinoshita, K., Harrison, S.C., Howard, J., and Hyman, A.A. (2008). XMAP215 is a processive microtubule polymerase. Cell *132*, 79–88.

Cannon, M.J., Williams, A.D., Wetzel, R., and Myszka, D.G. (2004). Kinetic analysis of beta-amyloid fibril elongation. Anal. Biochem. *328*, 67–75.

Cassimeris, L., Pryer, N.K., and Salmon, E.D. (1988). Real-time observations of microtubule dynamic instability in living cells. J. Cell Biol. *107*, 2223–2231.

Charlebois, B.D., Schek, H.T., 3rd, and Hunt, A.J. (2010). Nanometer-resolution microtubule polymerization assays using optical tweezers and microfabricated barriers. Methods Cell Biol. *95*, 207–219.

Charrasse, S., Schroeder, M., Gauthier-Rouviere, C., Ango, F., Cassimeris, L., Gard, D.L., and Larroque, C. (1998). The TOGp protein is a new human microtubule-associated protein homologous to the Xenopus XMAP215. J. Cell Sci. *111*, 1371–1383.

Chretien, D., Fuller, S.D., and Karsenti, E. (1995). Structure of growing microtubule ends: two-dimensional sheets close into tubes at variable rates. J. Cell Biol. *129*, 1311–1328.

Collins, S.R., Douglass, A., Vale, R.D., and Weissman, J.S. (2004). Mechanism of prion propagation: amyloid growth occurs by monomer addition. PLoS Biol. *2*, e321.

Demchouk, A.O., Gardner, M.K., and Odde, D.J. (2011). Microtubule Tip Tracking and Tip Structures at the Nanometer Scale Using Digital Fluorescence Microscopy. Cellular and Molecular Bioengineering *4*, 192–204.

Desai, A., and Mitchison, T.J. (1997). Microtubule polymerization dynamics. Annu. Rev. Cell Dev. Biol. *13*, 83–117.

Gardner, M.K., Bouck, D.C., Paliulis, L.V., Meehl, J.B., O'Toole, E.T., Haase, J., Soubry, A., Joglekar, A.P., Winey, M., Salmon, E.D., et al. (2008). Chromosome congression by Kinesin-5 motor-mediated disassembly of longer kinetochore microtubules. Cell *135*, 894–906.

Hill, T.L. (1986). Effect of fluctuating surface structure and free energy on the growth of linear tubular aggregates. Biophys. J. *49*, 1017–1031.

Howard, J., and Hyman, A.A. (2007). Microtubule polymerases and depolymerases. Curr. Opin. Cell Biol. *19*, 31–35.

Hunter, A.W., Caplow, M., Coy, D.L., Hancock, W.O., Diez, S., Wordeman, L., and Howard, J. (2003). The kinesin-related protein MCAK is a microtubule depolymerase that forms an ATP-hydrolyzing complex at microtubule ends. Mol. Cell *11*, 445–457.

Kerssemakers, J.W., Munteanu, E.L., Laan, L., Noetzel, T.L., Janson, M.E., and Dogterom, M. (2006). Assembly dynamics of microtubules at molecular resolution. Nature *442*, 709–712.

Mitchison, T., and Kirschner, M. (1984). Dynamic instability of microtubule growth. Nature *312*, 237–242.

Mitchison, T.J., and Kirschner, M.W. (1987). Some Thoughts On the Partitioning of Tubulin Between Monomer and Polymer Under Conditions of Dynamic Instability. Cell Biophys. *11*, 35–55.

Murphy, D.B., Johnson, K.A., and Borisy, G.G. (1977). Role of tubulin-associated proteins in microtubule nucleation and elongation. J. Mol. Biol. *117*, 33–52.

Northrup, S.H., and Erickson, H.P. (1992). Kinetics of protein-protein association explained by Brownian dynamics computer simulation. Proc. Natl. Acad. Sci. USA *89*, 3338–3342.

Oosawa, F. (1970). Size distribution of protein polymers. J. Theor. Biol. *27*, 69–86.

Pollard, T.D. (1986). Rate constants for the reactions of ATP- and ADP-actin with the ends of actin filaments. J. Cell Biol. *103*, 2747–2754.

Pryer, N.K., Walker, R.A., Skeen, V.P., Bourns, B.D., Soboeiro, M.F., and Salmon, E.D. (1992). Brain microtubule-associated proteins modulate microtubule dynamic instability in vitro. Real-time observations using video microscopy. J. Cell Sci. *103*, 965–976.

Rusan, N.M., Fagerstrom, C.J., Yvon, A.M., and Wadsworth, P. (2001). Cell cycle-dependent changes in microtubule dynamics in living cells expressing green fluorescent protein-alpha tubulin. Mol. Biol. Cell *12*, 971–980.

Schek, H.T., 3rd, Gardner, M.K., Cheng, J., Odde, D.J., and Hunt, A.J. (2007). Microtubule Assembly Dynamics at the Nanoscale. Curr. Biol. *17*, 1445–1455.

Shelden, E., and Wadsworth, P. (1993). Observation and quantification of individual microtubule behavior in vivo: microtubule dynamics are cell-type specific. J. Cell Biol. *120*, 935–945.

Skellam, J.G. (1946). The frequency distribution of the difference between two Poisson variates belonging to different populations. J.R. Stat. Soc. *109*, 296.

Stiffler, L.A., Ji, J.Y., Trautmann, S., Trusty, C., and Schubiger, G. (1999). Cyclin A and B functions in the early Drosophila embryo. Development *126*, 5505–5513.

Stukalin, E.B., and Kolomeisky, A.B. (2004). Simple growth models of rigid multifilament biopolymers. J. Chem. Phys. *121*, 1097–1104.

VanBuren, V., Cassimeris, L., and Odde, D.J. (2005). Mechanochemical model of microtubule structure and self-assembly kinetics. Biophys. J. *89*, 2911–2926.

VanBuren, V., Odde, D.J., and Cassimeris, L. (2002). Estimates of lateral and longitudinal bond energies within the microtubule lattice. Proc. Natl. Acad. Sci. USA *99*, 6035–6040.

Vasquez, R.J., Gard, D.L., and Cassimeris, L. (1994). XMAP from Xenopus eggs promotes rapid plus end assembly of microtubules and rapid microtubule polymer turnover. J. Cell Biol. *127*, 985–993.

Winey, M., Mamay, C.L., O'Toole, E.T., Mastronarde, D.N., Giddings, T.H., Jr., McDonald, K.L., and McIntosh, J.R. (1995). Three-dimensional ultrastructural analysis of the Saccharomyces cerevisiae mitotic spindle. J. Cell Biol. *129*, 1601–1615.